



UNIVERSITÀ POLITECNICA DELLE MARCHE
Repository ISTITUZIONALE

Experimental validation and uncertainty analysis of an innovative IoT infrared sensor for in-situ wall thermal transmittance measurement

This is the peer reviewed version of the following article:

Original

Experimental validation and uncertainty analysis of an innovative IoT infrared sensor for in-situ wall thermal transmittance measurement / Serroni, Serena; Arnesano, Marco; Martarelli, Milena; Revel, Gian Marco. - In: MEASUREMENT SCIENCE & TECHNOLOGY. - ISSN 0957-0233. - 34:12(2023). [10.1088/1361-6501/acf064]

Availability:

This version is available at: 11566/330033 since: 2024-05-21T10:37:31Z

Publisher:

Published

DOI:10.1088/1361-6501/acf064

Terms of use:

The terms and conditions for the reuse of this version of the manuscript are specified in the publishing policy. The use of copyrighted works requires the consent of the rights' holder (author or publisher). Works made available under a Creative Commons license or a Publisher's custom-made license can be used according to the terms and conditions contained therein. See editor's website for further information and terms and conditions.

This item was downloaded from IRIS Università Politecnica delle Marche (<https://iris.univpm.it>). When citing, please refer to the published version.

(Article begins on next page)

29 **Nomenclature**

30

31 *ASHRAE American Society of Heating, Refrigerating and Air-Conditioning Engineers*

32 *AVGM Average Method*

33 *BIM Building Information Model*

34 *$c(x_i)$ Sensitivity Coefficient of the x_j input estimate*

35 *cdf cumulative density function*

36 *ε Emissivity*

37 *GUM Guide to the expression of Uncertainty in Measurement*

38 *h Heat transfer coefficient*

39 *h_c Convective heat transfer coefficient*

40 *HF Heat Flux*

41 *HFM Heat Flux Meter*

42 *h_r Radiative heat transfer coefficient*

43 *IEQ Indoor Environmental Quality*

44 *IoT Internet of Things*

45 *IRT Infrared Thermography*

46 *IR Infrared*

47 *L Component thickness*

48 *M Number of trials*

49 *MCM Monte Carlo Method*

50 *pdf probability density function*

51 *PM Particulate Matter*

52 *q heat flux*

53 *Q_{cond} Conductive heat flux*

54 *Q_{conv} Convective heat flux*

55 *Q_{rad} Radiative heat flux*

56 *RH Relative Humidity*

57 *ROI Region Of Interest*

58 *σ Stefan-Boltzmann constant*

59 *S_i Sensitivity index with respect to the x_i input estimate*

60 *T_a Air temperature*

61 *T_{atm} Atmosphere temperature*

- 62 T_e Outdoor air temperature
- 63 T_i Indoor air temperature
- 64 T_{refl} Reflected temperature
- 65 T_{si} Indoor surface temperature
- 66 T_{tot} Total temperature
- 67 $u(x_i)$ Standard uncertainty associated with the input estimate x_i
- 68 $u(y)$ Uncertainty of the output y
- 69 V_{xi} Variance due to the perturbation of the model associated with the input estimate x_i
- 70 V_{tot} Total variance of the output due to the perturbation of the model
- 71
- 72
- 73
- 74
- 75
- 76
- 77
- 78
- 79
- 80
- 81
- 82
- 83
- 84
- 85
- 86
- 87
- 88
- 89
- 90
- 91
- 92
- 93
- 94
- 95

97 1. Introduction

98 Buildings are one of the major contributors to global energy consumption, therefore improving building energy
99 efficiency has become a strategic and crucial issue. In [1] and [2] it was reported that roughly 40% of global
100 energy is consumed by buildings. Particularly in [1] the authors pointed out that the difficulty in reducing this
101 percentage lies in the gap between the energy performance predicted in the project phase and the actual energy
102 performance measured [3]. Over the last years, various approaches have been used to monitor and improve
103 building energy performance. In [4], for example, the authors proposed the long-term observation of electric
104 parameters combined with methods and algorithms that can evaluate buildings' ageing process and an
105 intelligent control that further enables local energy management on the part of consumers as well as
106 consumption management in smart grids. In [2] measurement and control were extended also to health and
107 comfort monitoring for a smart building concept. Whereas in [5] a machine learning approach was presented
108 with the purpose of predicting the energy performance (heating load and cooling load) of residential structures.

109 One of the most critical elements affecting the heating and cooling energy consumption in built environments
110 is the thermal performance of their envelopes [6][7]. When the stratigraphy of the envelope component is
111 known, the thermal transmittance (U-value) can be determined using the EN ISO 6946 standard [8] with an
112 uncertainty range of 5–50%, or it can be calculated using laboratory testing in line with the EN ISO 8990
113 standard [9]. Both the methods have the limitation that, when building elements are unknown, for the
114 implementation of the standards, core boring or endoscopic tests, which are destructive, or alternatively
115 laboratory tests, which are not always feasible, are required.

116 The ISO 9869-1 standard [10] defines a method for in-situ thermal transmittance measurements which makes
117 use of contact sensors, e.g., thermocouples and HFMs (Heat Flux Methods). However, these are a local
118 measurement which are often not indicative of the dynamic thermal response of a whole wall, particularly in
119 prefabricated panels with a complex internal structure. In-situ measurements are also affected by
120 environmental conditions [11], which, however, can be statistically cancelled out if the measurement duration
121 is longer than the typical daily environmental cycle, which is the reason why the standard requires a test to last
122 at least 72 hours. The thermal conductivity measured using an HFM is also affected by radiative heat losses,
123 as evidenced in [12]. This interfering input cannot be neglected if the heat flow is not purely mono-directional.
124 To make sure that this hypothesis is verified, the mounting position of the HFM needs to be identified a priori.

125 In [13] the authors described an alternative to the method defined in ISO 9869-1 which has two upgrades:

- 126 - an additional HFM on the external surface of the building façade, besides the sensor installed on the
127 interior side as suggested by the standard;
- 128 - the calculation of thermal transmittance from the heat flux obtained from the average of the heat fluxes
129 measured by the two sensors.

130 These methods allow a reduction of both measurement time (from the minimum required 72 hours down to 24
131 hours) and uncertainty of the thermal transmittance measurement (from 8% to 5%).

132 Nevertheless, environmental conditions remain an interfering input when assessing thermal transmittance. To
133 reduce their influence on heat flow and temperature measurements, in [11] the authors proposed to apply an
134 artificial thermal load produced by a heating box to the façade wall where the sensors are mounted. On the one
135 hand, the approach reaches an accuracy of 4.4–7.5%. On the other hand, however, the procedure is extremely
136 time consuming. A hybrid method to improve the robustness of U-value estimation of building envelopes was
137 proposed in [14]. The method integrated the experimental data measured by means of heat flux sensors with
138 the U-value calculation of wall surface via a mono-dimensional nodalisation of the wall itself. Numerical and
139 experimental data were exploited in an optimisation problem based on the minimisation of the RMS values of
140 the deviations of both the calculated and experimental heat fluxes. This method can be applied to any kind of
141 wall, including those with a complex stratigraphy, since it makes it possible to assess an equivalent
142 conductivity and calculate wall conductance and its equivalent thermal capacity.

143 All the methods described above make use of contact sensors (thermocouples and heat flow meters), which
144 limit the evaluation of thermal transmittance to punctual values in the space. As a consequence, due to the
145 difficulty in accounting for the potential existence of thermal bridges in the test wall, the U-value computed is
146 underestimated. Due to this, the use of infrared sensors for measuring the U-value has recently been
147 investigated, for example in [15]. In fact, thermal cameras, which make use of IR sensors, make it possible to
148 frame large portions of building envelopes and identify regions with unusual thermal behaviour (such as local
149 thermal bridges, regions with excessive moisture content), which can be and excluded from further research.
150 The primary drawback of this approach is that it has a poor repeatability index for light walls and super-
151 insulated constructions because IR sensors are highly dependent on ambient factors (external radiation, wind),
152 which results in low accuracy values with an uncertainty of up to 20% [16]. Some studies suggested using
153 thermal cameras to estimate thermal transmittance when the test wall is under quasi steady-state ([17], [18])
154 or steady-state ([19]) conditions by detecting heat flow and surface temperature. However, this kind of
155 conditions are impractical and can very rarely be reproduced in real environments. Other works overcame this
156 difficulty by considerably increasing test durations to reduce the error related to the variability of
157 environmental conditions ([20], [21], [22]).

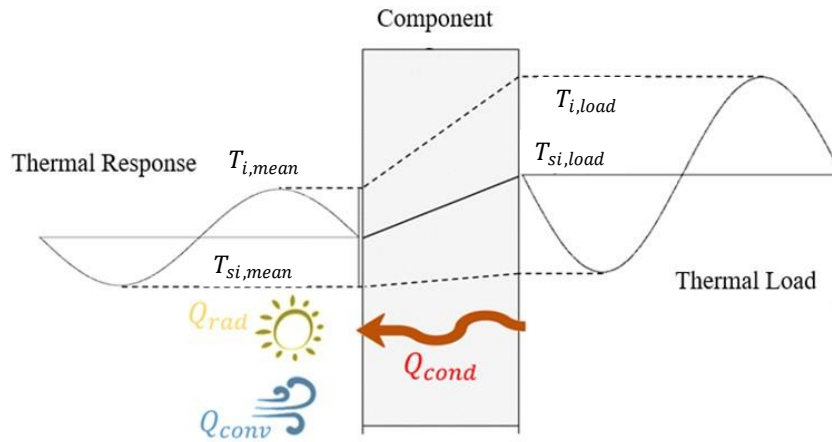
158 The ISO 9869-2-2018 standard regulates the use of thermography for the estimation of the U-value in built
159 environments [23]. The standard also introduces a method to calculate the heat transfer coefficient (h) in-situ,
160 which is considered critical in real settings. The methods used to calculate h are the IR camera and the active
161 heat flux meter. To estimate thermal transmittance, the standard advises taking measurements at night for a
162 minimum of three consecutive days. Alternatively, measurements may end once thermal transmittance,
163 computed using the moving average technique, converges to a constant value with a variance of less than 10%.

164 The system and approach proposed in this study are based on the estimation of the U-value of a building
165 element which is derived from the indoor surface temperature obtained using an IoT system, Comfort Eye
166 [24][25]. This study intends to investigate and delve further into Comfort Eye's functionality, which typically
167 makes it possible to measure the data required for Indoor Environmental Quality (IEQ). The Comfort Eye
168 sensor consists of two nodes, i.e. a ceiling node with an infrared sensor and a desk node with sensors for the
169 measurement of environmental parameters. When in a scanning mode, the IR sensor can frame the whole walls
170 of the room where it is installed. In the case of façade walls, it enables the continuous monitoring of the thermal
171 dynamic behaviour of the walls. The approach, which was developed within the European project BIMSPEED
172 [26], is based on the estimation of the heat flow from the indoor surface temperature obtained using the ceiling
173 node and was tested in a real setting using an HFM as a reference. The system was installed in the laboratory
174 at the Polytechnic University of Marche in January 2022. An uncertainty analysis based on Monte Carlo
175 simulations was also performed to analyse the overall uncertainty of the method as well as the impact of the
176 uncertainty of the input variables on the U-value measurement output [27].

177 **2. Methodology**

178 **2.1 Transmittance calculation**

179 IR thermography makes it possible to assess the surface temperature of an object by measuring the distribution
180 of the radiant thermal energy (radiant heat transfer) emitted by the hot surface. If the object is a building
181 element like a façade wall experiencing a thermal gradient between its internal and external surface, the surface
182 temperature can be related to the thermal properties of the wall and specifically to its thermal transmittance.
183 To analytically quantify this relation, an understanding of the different types of heat transfer arising between
184 the surface of the building element and the IR sensor is required [28]. A generic component of thickness L (in
185 m) as sketched in Figure 1 is considered and exposed to a thermal load (on the right of the sketch) that induces
186 a surrounding air temperature of $T_{i,load}$ and a wall surface temperature of $T_{si,load}$. If the temperatures of the
187 air and wall surface on the left of the sketch are different, due to the thermal gradient, the component
188 experiences a conductive heat flux through the material (Q_{cond}) which depends on the transmittance properties
189 of the material itself. The temperature of the wall surface on the left of the sketch ($T_{si,mean}$) depends on the
190 conductive heat transfer and it is measured by the IR camera sensor, which is also sensitive to the radiant and
191 convective flows (Q_{rad} and Q_{cond}) between the wall and the sensor itself [29].



193 *Figure 1 Thermal dynamic behaviour of a building component (wall)*

194 The equilibrium condition between the building component and its surrounding air is obtained when the
 195 conductive heat flux is equal to the sum of the radiative and convective heat fluxes, as expressed in Equation
 196 (1):

$$Q_{cond} = Q_{conv} + Q_{rad} \quad (1)$$

197

198 where Q_{cond} is the conductive heat flux and Q_{conv} , and Q_{rad} are the convective and radiative fluxes,
 199 respectively (W/m^2). With regards to the convective heat flux states:

$$Q_{conv} = h_c \times (T_i - T_{si}) \quad (2)$$

200

201 where h_c is the convective heat transfer coefficient ($W/(m^2K)$), T_i the indoor air temperature (K), and T_{si} the
 202 surface temperature (K). With regards to the radiative heat flux states:

$$Q_{rad} = h_r \times (T_i - T_{si}) \quad (3)$$

203

204 where h_r is the radiative heat transfer coefficient ($W/(m^2K)$).

205 According to Acikgoz et al. [30], h_r , which is calculated using Equation (4), has a constant value at low
 206 temperatures ($-10^\circ C$ to $50^\circ C$):

$$h_r = \varepsilon \times \sigma \times (T_i^4 - T_{si}^4) / (T_i - T_{si}) \quad (4)$$

207

208 where σ is the Stefan-Boltzmann constant ($5.67 * 10^{-8} W/m^2K^4$) and ε is the emissivity of the wall surface.

209 The coefficient h_c can be calculated using analytical, numerical, or experimental approaches. The latter are
 210 the primary way for calculating h_c . However, empirical equations are influenced by a wide variety of
 211 conditions. With regards to natural convection, h_c can be expressed using Equation (5) for every surface
 212 [31][32].

$$h_c = C \times \Delta T^n \quad (5)$$

213

214 where C and n are constants and can be found in literature, and $\Delta T = T_i - T_{si}$. Different authors provide
 215 different values which are listed in , respectively.

216 Table 1.

217 For vertical surfaces, in ISO 6946 [8] and ISO 9869 [10] h_c is supposed to be 2.5 W/m²K and 3.00 W/m²K,
 218 respectively.

219 *Table 1 Values of C and n defined by different authors and used to calculate the h_c coefficient [32]*

Authors	h_c (W/(m ² K))
Khalifa et al.	$2.07 \times \Delta T^{0.230}$
Awbi et al.	$1.49 \times \Delta T^{0.345}$
Michejev	$1.55 \times \Delta T^{0.330}$
King	$1.51 \times \Delta T^{0.330}$
Nusselt	$2.56 \times \Delta T^{0.250}$
Heilman	$1.67 \times \Delta T^{0.250}$
Wilkens et al	$3.04 \times \Delta T^{0.120}$
ASHRAE	$1.31 \times \Delta T^{0.330}$
ISO 9869	3.00
ISO 6946	2.5

220

221 The IR sensor provides the T_{si} measurement, and therefore it makes it possible to estimate the radiant and
 222 convective fluxes (by Equation (2) and (3)). Hence, the U-value is calculated with the moving average method
 223 (AVGM) according to Equation (6):

224

$$U = \sum_{j=1}^N (Q_{rad} + Q_{conv}) / \sum_{j=1}^N (T_i - T_e)_j \quad (6)$$

225

226 where T_e is the outdoor air temperature, T_i is the indoor air temperature, and the index j counts the running
 227 measures considered in the moving average process. T_i is provided by Comfort Eye's desk node, and T_e is
 228 measured by a weather station. The reference U-value from the HFM measurement is calculated using the
 229 following equation:

$$U = \sum_{j=1}^N q_j / \sum_{j=1}^n (T_i - T_e)_j \quad (7)$$

230

231 where q_j is the heat flux and T_i , T_e are the indoor and outdoor air temperature, respectively, while index j
 232 counts the individual samples.

233 To consider the small variability of the quantities measured, the final U-value is calculated as the mean of the
 234 last 10 samples for both models, i.e. the HFM model and the IR model.

235 2.2 Comfort Eye: IR sensor

236 Comfort Eye [33] is an IoT and low-cost system which makes it possible to assess the thermal dynamic
 237 behaviour of a whole wall through the real-time and continuous thermal monitoring of the building. The sensor
 238 consists of 2 nodes, i.e., a ceiling node with an infrared sensor, and a desk node that measures relative humidity
 239 (RH), CO_2 , indoor air temperature (T_i), and Particulate Matter (PM) using two sensors, namely Sensirion
 240 SPS30, which measures PM , and Sensirion SCD30, which measures T_i , RH , and CO_2 in a single point. The
 241 ceiling node that detects the wall's inside surface temperature (T_{si}) is Comfort Eye's key innovative aspect. It
 242 is a 2-axes rotating 3D thermal scanner (MLX90621) that produces thermal maps of interior surface
 243 temperatures. The IR system consists of a 16x4 thermopile array; thus, each frame captured has a map of 64
 244 wall temperatures and a field of view of 60x16°. Therefore, at the distance of one meter from the sensor, the
 245 area scanned is of 1.15 x 0.56 m. The device entails a custom mainboard with a microcontroller, programmed
 246 with dedicated firmware, to perform the automatic scanning of all the room's surfaces by controlling the
 247 horizontal and vertical movements of servos. All the specifications of the sensors are given in **Errore.**
 248 **L'origine riferimento non è stata trovata..**

249

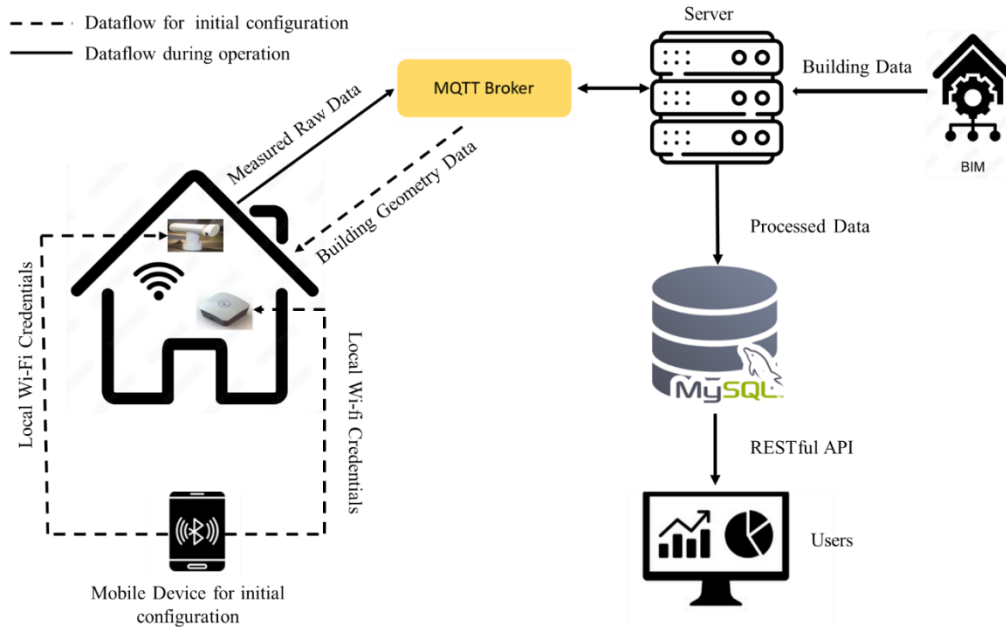
Table 2 Specifications of Comfort Eye's sensors (Ceiling node and Desk node)

Sensors	Range	Accuracy	Repeatability
IR sensor	-20 °C – 300 °C	± 1 °C	/
CO ₂	0-40000 ppm	± (30ppm + 3%MV)	±10 ppm
RH	0%-100%	±3%RH	±0.1%RH
T_i	-40 °C-70°C	± (0.4 + 0.023 × (T[°C]-25°C))	±0.1°C
PM _{2.5}	0-1000(µg/m ³)	±10 (µg/m ³)	/

PM100-1000($\mu\text{g}/\text{m}^3$) $\pm 10(\mu\text{g}/\text{m}^3)$ /

250

251 In Figure 2, the IoT architecture of the entire system is illustrated.



252

253 *Figure 2 Comfort Eye's general architecture. The system is composed of a ceiling node with an infrared sensor that*
254 *scans the whole walls of the room and a desk node that acquires environmental parameters. The configuration and*
255 *operation dataflows are managed by means of a dedicated architecture that integrates mobile devices and a remote*
256 *server for data processing.*

257

258 Once the two nodes are installed in the building to be tested, the Wi-Fi network credentials are sent via
259 Bluetooth, the nodes then connect to the local network, and the data are sent to the server, processed, and stored
260 in a MySQL database. The entire process is real-time and continuous. The communication module used is the
261 PyCOM W01, which implements Bluetooth Low Energy and supports the Message Queuing Telemetry
262 Transport (MQTT) protocol. A dashboard was developed for the evaluation of thermal performance and data
263 exploration. The dashboard is a web app that is accessible via any browser. Core data processing is served by
264 a RESTful API (Application Programming Interface) running on the server and retrieved with a standard GET
265 request.

266 The thermographic images are corrected taking into account the wall geometry, which, if available, can be
267 automatically extracted from the Building Information Model (BIM), the reflected temperature and the
268 emissivity of the wall. A detailed description of the IR scan sensor can be found in [33], while in [34] a
269 thorough description of the IoT architecture of the system is provided.

270

271

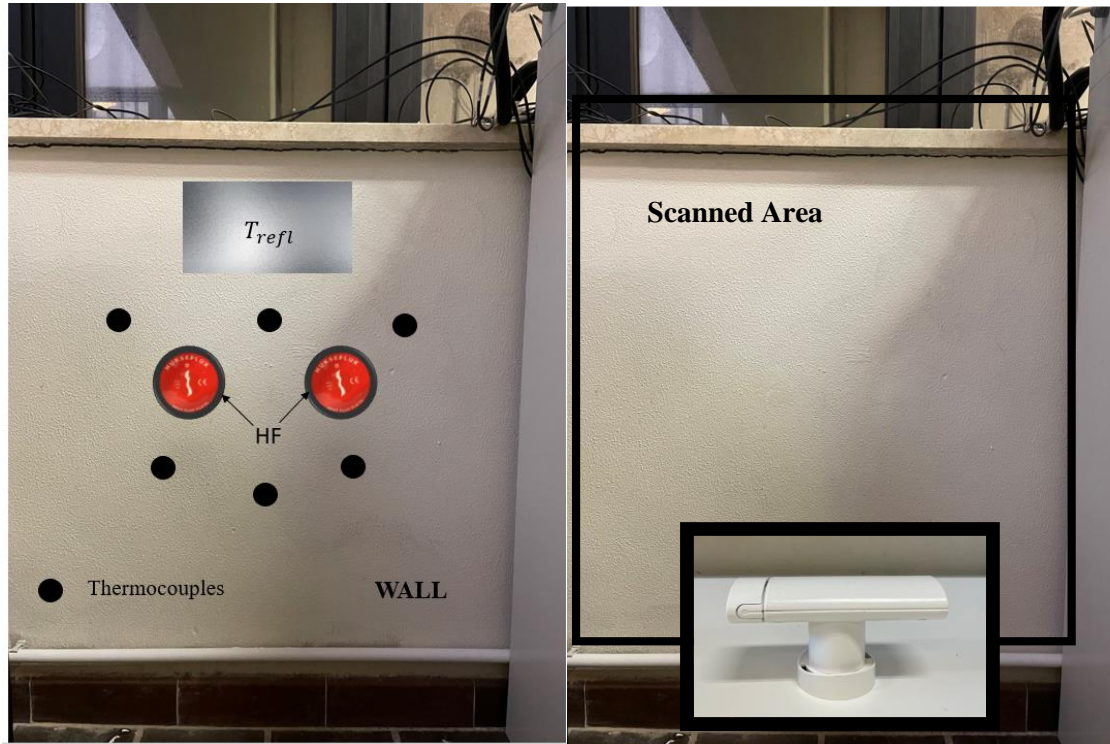
3. Experimental test setup

272 The methodology presented was validated in a real environment using an HFM as a reference. The system was
273 installed in a room of the laboratory at the Polytechnic University of Marche in January 2022. The wall
274 analysed has a thickness of 0.40 cm and is composed of three layers, i.e. a concrete layer of 0.15 cm, an
275 insulation layer of 0.10 cm, and a second concrete layer of 0.15 cm.

276 The sensors were configured to collect data every four minutes. The measuring campaign was conducted in
277 the period between 2nd February 2022 and 3rd March 2022 on a wall with windows that were not directly
278 exposed to solar radiation. The exterior surface of the wall overlooks onto an atrium and is shielded from
279 weather conditions by the atrium's roof. In the period considered, the inside environment was heated by
280 radiators from 7:00 a.m. until 9:00 p.m. The measurements were carried out in accordance with ISO 9869-1
281 [10] for the HFM method and ISO 9869-2 [23] for the IR method. In particular, for the HFM measurements
282 the following protocol was considered:

- 283 • the heat flux sensor was not positioned in proximity to the components with high thermal conductivity;
- 284 • the surface examined was shielded from weather conditions (rain, wind, solar radiation);
- 285 • the time intervals between data acquisitions were less than 30 minutes;
- 286 • the measuring time for stable boundary temperatures exceeded 72 hours.

287 As far as the IR method is concerned, in accordance with ISO 9869-2, the experimental data were considered
288 valid only when the difference between indoor and outdoor air temperatures was at least 10° C. The IR
289 scanning system (Comfort Eye) was installed in front of the wall under test with the two fixed rotary axes to
290 measure the superficial temperature of the wall. Comfort Eye's desk node, which was used to measure the
291 internal temperature, was placed in an environment-representative location away from heat sources, sunlight,
292 direct ventilation, and other factors that could interfere with the measurements. As a reference system, six
293 Type T thermocouples were mounted on the internal surface of the wall, so as to monitor the surface
294 temperatures. In addition, a thermocouple was placed inside the room and a further one outside the room, so
295 as to measure the room's outdoor and indoor air temperatures. Two heat flux transducers (HFP01 sensor based
296 on thermopile [35]) were mounted on the internal surface of the wall to monitor the thermal flow through its
297 thickness. A thermocouple was mounted on a piece of low-emissivity aluminium foil placed on the surface
298 scanned by the infrared camera to measure the reflected temperature and correct the measured temperature
299 from the energy reflected by the environment. The emissivity of the wall was calculated using the reference
300 method, i.e. by installing a 3M insulating tape with known emissivity of 0.95 on the wall. The U-value was
301 calculated in the same Region of Interest (ROI) of the HFM (Figure 3), therefore considering only the values
302 relating to the wall without the thermal bridge.



304 *Figure 3 Experimental setup. The figure on the left shows the wall analysed using the reference system (heat flow meter*
 305 *and thermocouples) and the aluminium foil to measure the reflected temperature. The figure on the right shows the wall*
 306 *analysed using Comfort Eye*

307

308 The temperature of the wall surface (T_{si}) scanned by Comfort Eye's IR sensor was corrected by applying
 309 Equation (8):

$$T_{si}^4 = \frac{1}{\varepsilon\tau} T_{tot}^4 - \frac{1-\varepsilon}{\varepsilon} T_{refl}^4 - \frac{1-\tau}{\varepsilon\tau} T_{atm}^4 \quad (8)$$

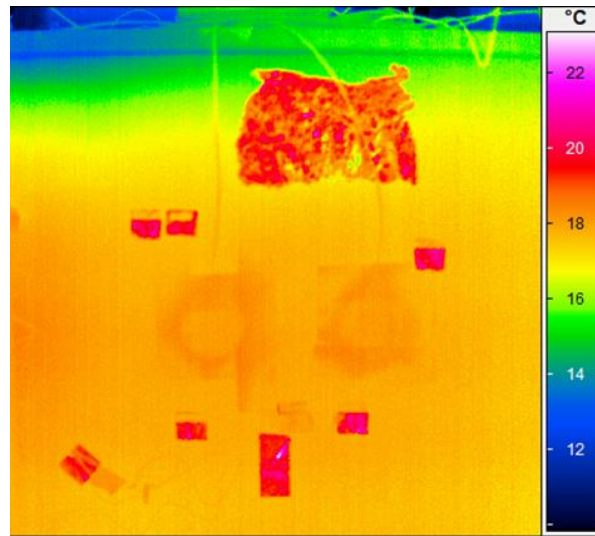
310

311 where τ is the constant atmospheric transmission coefficient, which is assumed to be equal to 0.99, ε the
 312 emissivity of the surface being measured, T_{refl} the reflected temperature computed by measuring the
 313 contribution of the opposite surface with an ε set equal to 1, T_{tot} the raw value of the total temperature detected
 314 by the IR sensor of the ceiling node, and T_{atm} the temperature of the atmosphere, which is considered to be
 315 equal to indoor air temperature (T_i).

316 The correction equation is necessary because the raw values detected by the IR sensor can be affected by
 317 various factors, such as the emissivity and reflectivity of the surface being measured, as well as the temperature
 318 of the atmosphere. By applying this equation in the pre-processing phase, it was possible to obtain a more
 319 accurate temperature reading of the wall surface, which is important in studies related to thermal transmission
 320 calculation.

321 Figure 4 shows a thermogram acquired during the test performed to measure the ϵ of the wall using InfraTec-
322 Head 980. The emissivity obtained was 0.95.

323



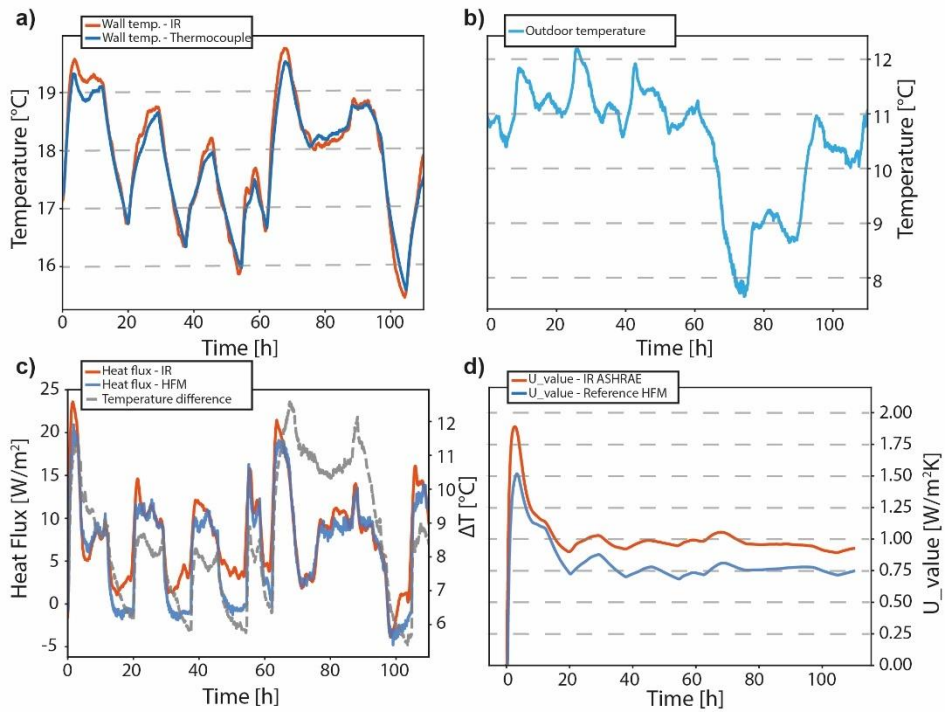
324 *Figure 4 Thermogram of the wall acquired using the InfraTec Head 980 IR camera for the estimation of wall emissivity*

325 **4. Results**

326 The outcomes of the tests conducted are reported in Figures 5-6-7, which compare the thermal transmittance
327 calculated using both the methodologies, i.e. the HFM and Comfort Eye with the U-values calculated using
328 the h_c coefficient given by ASHRAE (American Society of Heating, Refrigerating and Air-Conditioning
329 Engineers) in three different time windows (I, II, III). The analysis was initially performed considering the
330 h_c values given by the different authors (Table 1). In previous work [24] the authors showed that optimal
331 results are obtained when using the value of h_c defined by Wilkers. However, under the conditions of the study
332 here presented, the analysis demonstrated that the h_c coefficient given by ASHRAE makes it possible to obtain
333 the best results. The uncertainty analysis discussed in the next section confirms the selection of the model
334 based on the h_c coefficient calculated by ASHRAE.

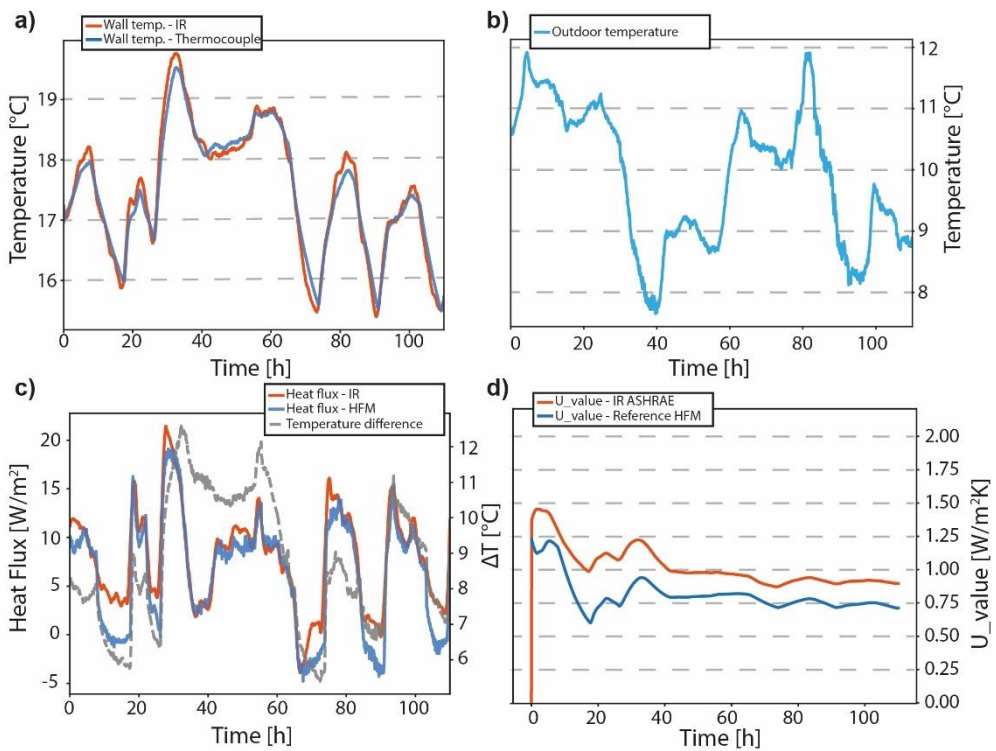
335 In details, Figure 5Figure 6Figure 7 show (a) the trend of the indoor surface temperature T_{si} measured using
336 Comfort Eye's IR sensor and a Type T thermocouple, and (b) the external temperature T_e measured with the
337 Type T thermocouple used to calculate the thermal transmittance in the period considered. The figures also
338 show (c) the trend of the heat flux calculated using Comfort Eye and the HFM together with the corresponding
339 temperature difference $\Delta T = T_i - T_e$, and (d) the trend of the U-value estimated with both Comfort Eye and
340 the reference method based on HFM. Three different 120 h time windows are reported in the three figures to
341 demonstrate the repeatability of the model applied. According to ISO 9869-2, the difference between indoor
342 and outdoor air temperature ΔT must be greater than 10 °C for at least 50 % of the time window considered.

343



345

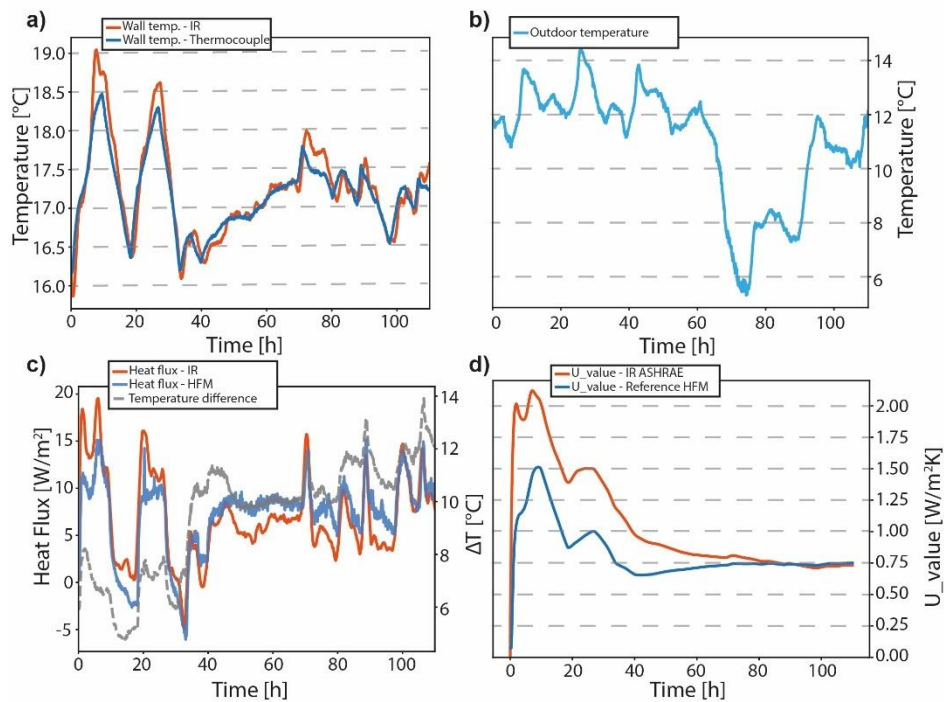
346 *Figure 5 Time window I - trends: a) indoor wall temperature measured using the IR sensor (Comfort Eye) and the*
 347 *reference thermocouple, b) external temperature, c) heat flux obtained using the IR sensor (Comfort Eye) and the HFM*
 348 *with the corresponding ΔT , d) U-value estimated using the IR sensor (Comfort Eye) and the HFM*



349

350 *Figure 6 Time window II - trends: a) indoor wall temperature measured using the IR sensor (Comfort Eye) and the*
 351 *reference thermocouple, b) external temperature, c) heat flux obtained using the IR sensor (Comfort Eye) and the HFM*
 352 *with the corresponding ΔT , d) U-value estimated using the IR sensor (Comfort Eye) and the HFM*

353



355 *Figure 7 Time window III - trends: a) indoor wall temperature measured using the IR sensor (Comfort Eye) and the*
 356 *reference thermocouple, b) external temperature, c) heat flux obtained using the IR sensor (Comfort Eye) and the HFM*
 357 *with the corresponding ΔT , d) U-value estimated using the IR sensor (Comfort Eye) and the HFM*

358 Considering the different time windows, the result obtained in time window I (Figure 5) is a U-value of 0.92
 359 W/m²K against the U-value of 0.74 W/m²K measured using the HFM. In time window II (Figure 6) the result
 360 is a U-value of 0.89 W/m²K against the U-value of 0.71 W/m²K measured using the HFM, while in time
 361 window III (Figure 7) the result is a U-value of 0.73 W/m²K against the U-value of 0.75 W/m²K estimated
 362 with the HFM.

363 5. Measurement Model

364 The primary objective of this study is to develop a cutting-edge mathematical model for measuring thermal
 365 transmittance (U-value) using an innovative IoT system called Comfort Eye. This system enables continuous
 366 and real-time monitoring, surpassing the limitations of conventional methods. The Comfort Eye system
 367 comprises two nodes: a rotating two-axis infrared (IR) sensor typically installed at the ceiling's center to scan
 368 all walls of the room, in this study, the IR node is positioned with fixed rotating axes at 1-meter distance from
 369 the wall under analysis, the area scanned is of 1.15 x 0.56 m, and a desk node for measuring environmental
 370 parameters. The desk node is strategically positioned away from heat sources and direct solar radiation. The
 371 IR sensor captures surface temperature data T_{si} , critical for U-value calculation, and the desk node records
 372 indoor temperature T_i , another essential input for the model. External temperature can be measured by a
 373 thermocouple or extracted from an external weather station via an API service T_e . The emissivity of the wall
 374 (ϵ) is determined using InfraTec-Head 980 and a reference method involving the installation of a 3M insulating
 375 tape with a known emissivity of 0.95. The sensors were configured to collect data every four minutes. The
 376 measuring campaign was conducted in the period between 2nd February 2022 and 3rd March 2022 in order to

377 satisfy the requirements defined by ISO 9869-1 [10] and ISO 9869-2. The mathematical model employs
378 various input variables, including corrected surface temperature T_{si} , indoor temperature T_i , external
379 temperature T_e , and emissivity ε , to calculate the U-value.

380

381 Mathematical Model:

382 The Comfort Eye mathematical model is derived from equations 2 to 6, which consider the essential input
383 variables for U-value calculation. The corrected surface temperature is obtained through meticulous
384 processing, considering factors like emissivity and geometry (Equation 8). The desk node records continuous
385 indoor temperature readings, while the external temperature is measured by the thermocouple or obtained from
386 an external weather station. The emissivity of the wall is determined using a reliable reference method. With
387 these variables and relevant constants (σ , C, n), equations 4 and 5 yield h_r and h_c . Equations 2 and 3 are then
388 applied to determine heat flux (Q_{cond} and Q_{rad} , respectively). The final U-value is calculated using equation
389 6, incorporating Q_{cond} , Q_{rad} , and indoor and outdoor temperatures (T_i, T_e)

390

391 Uncertainty Analysis:

392 To evaluate measurement uncertainty, the Monte Carlo Method (MCM) is employed. The MCM approach
393 generates uncertainty distributions for each input variable without direct mathematical model ($T_{si}, T_i, T_e, \varepsilon$),
394 considering standard deviations obtained from datasheets or previous studies. Through this simulation, the
395 uncertainty in U-value measurements is determined, aiding in understanding the measurement accuracy of the
396 model under real environmental conditions. The results demonstrate the influence of different variables on
397 measurement uncertainties, with temperature-related variables playing a significant role.

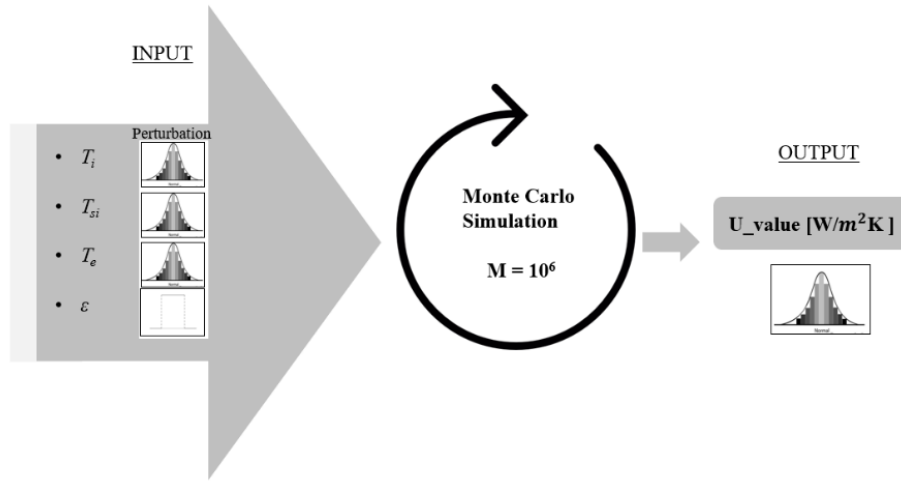
398

399

400 **6. Uncertainty estimation and sensitivity analysis**

401 **6.1 Monte Carlo analysis**

402 In this study, a method for the evaluation of the effect of the uncertainty related to input variables on U-value
403 calculation is applied. When reporting the result of the measurement of a physical quantity, it is mandatory to
404 provide a quantitative indication of the quality of the result, so that its reliability can be assessed. The Guide
405 to the Expression of Uncertainty in Measurement (GUM) [27] defines the uncertainty assessment of a
406 numerical model by using a Monte Carlo Method (MCM) [37](Figure 8).



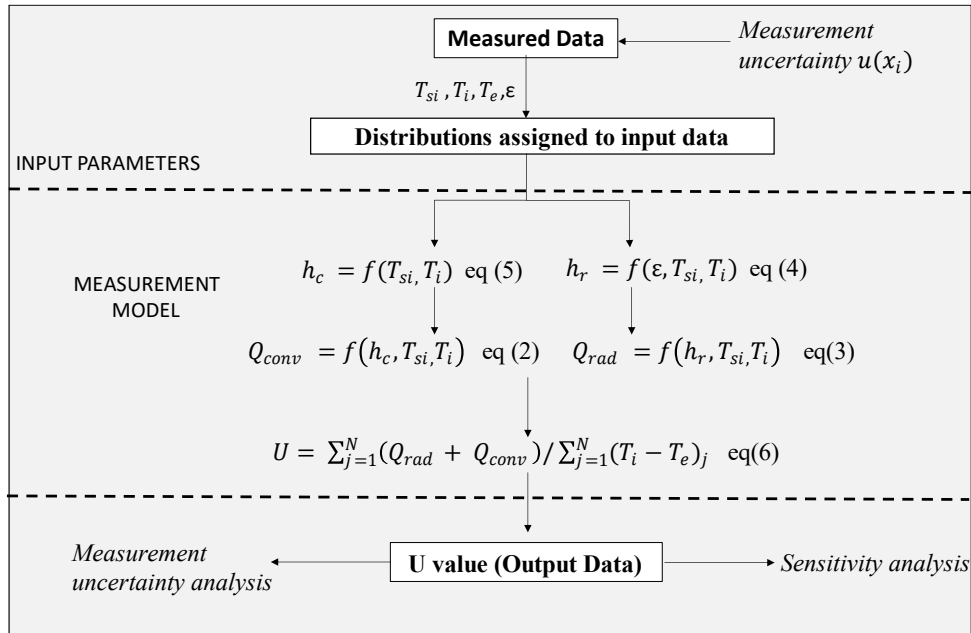
407
408 *Figure 8 Input variables (T_{si} , T_i , T_e , ε) for the MCM*

409 This approach is based on the generation of uncertainty distributions of data associated to each input of the
410 model, to have a statistical distribution of the variables from which the uncertainty of the model can be
411 evaluated in terms of standard deviation. For each measured data used as input of the model, the uncertainty
412 of the specific sensor was considered and a Monte Carlo simulation was performed by generating random
413 numbers in these uncertainty ranges by assuming a uniform or Gaussian distribution. The uncertainty of the
414 model in terms of standard deviation was calculated by perturbing all the input variables simultaneously. In
415 the study here presented, the sensitivity coefficients were calculated according to Annex B of JCGM 101:2008
416 by perturbing the value of each input parameter while keeping all the other parameters constant and then
417 propagating the uncertainty through the model to calculate the resulting uncertainty in the output.

418 The conceptual description of the uncertainty estimation via the Monte Carlo method and the sensitivity
419 analysis for the thermal transmittance measurement model are summed up in Figure 9. It consists of inputs
420 directly measured by different sensors and a mathematical model based on the equations from (2) to (6)
421 presented in Section 2.1. The inputs are:

- 422 1. the surface temperature T_{si} , measured by the ceiling node of the comfort eye,
423 2. the indoor temperature T_i , measured by the desk node of the comfort eye,
424 3. the external temperature T_e , measured by a thermocouple applied to the wall external surface or
425 retrieved from nearby weather stations
426 4. the emissivity of the wall (ε) which must be known or measured on purpose.

427 The Monte Carlo method has been employed for propagating uncertainties of variables that cannot be explicitly
428 modelled using mathematical equations. When calculating the thermal transmittance (U-value), the only
429 variables without a direct mathematical model are T_i , T_{si} , T_e , ε . Additionally, Figure 9 enhance the clarity of
430 the measurement model and define the interrelations among the variables.



431

432

Figure 9 Model of Measurement of the thermal transmittance using IR sensor

433

The uncertainty propagation method [27] was used to evaluate the deviation of the U-value measured by means of Comfort Eye's IR system with respect to the value obtained with the HFM method, which was taken as a reference in this study. It is important to underline that the uncertainty values estimated in this analysis should not be considered as the absolute uncertainty of the tool but rather as a discrepancy with respect to the reference HFM, which, in addition, includes its own component of uncertainty. The variables involved were assumed to be statistically uncorrelated. MCM provides a generic method for numerically approximating the cumulative density function (*cdf*) of the output of a specific variable $y = f(x)$. MCM is based on the concept that any sample of x_i (input quantity) selected from a predetermined distribution can be employed. Consequently, by randomly sampling each input x_i , it is possible to estimate a potential output y outcome and its related uncertainty using the corresponding probability distribution function (*pdf*).

443

In the analysis presented, MCM consisted in the following steps:

444

1) the number of trials, N , was fixed to 10^6 , which provides a 95% coverage interval, as described in the GUM supplement. The greater N , the higher the expected convergence of outcomes;

445

446

2) M vectors x_i , $i = 1, \dots, M$, in this case $M = 4$, were derived by randomly picking from the *pdfs* of each input quantity, i.e. $[T_i, T_{si}, T_e, \epsilon]$ for the IR model (Comfort Eye) and $[T_i, T_e, q]$ for the HFM model, to obtain potential inputs to be correlated to x_i ;

447

448

3) for each of the vectors obtained in point two, the analogous output y (U-value) was computed using both the models considered in this work, i.e. i) the HFM model, ii) the IR model with Comfort Eye using the h_c values calculated by ASHRAE and Wilkers. The dimension of the output was therefore M ;

449

450

4) the representation G of the distribution functions of Y was generated starting from the set of M outputs of Y ;

451

452

453

454

- 455 5) G was used to obtain the appropriate coverage region of Y;
456 6) the sensitivity coefficients $c_i(x_i)$ were calculated.

457 Tables 3, 4 and 5 show the standard uncertainty $u(x_i)$, the uncertainty of the output $u_i(y)$ and the
458 sensitivity coefficients $c(x_i)$, which are the final output of the analysis.

459 Equation (9) was used to calculate the sensitivity coefficients $c(x_i)$:

$$c(x_i) = \frac{u_i(y)}{u(x_i)} \quad (9)$$

460 In accordance with the concept of maximum entropy, since the sole information on the quantity X was its
461 range limit, a rectangular distribution was used for ε , with an upper limit $b = 0.97$ and a lower limit $a = 0.93$.
462 Whereas, a Gaussian distribution was used for T_{si}, T_i, T_e , since the best estimate x and associated standard
463 uncertainty $u(x)$ were the sole information on the quantity X. The uncertainty of T_e (Type T Thermocouple)
464 was derived from the datasheet of the sensor, while the uncertainties of T_i, T_{si} , were obtained from the analyses
465 carried out in previous works [33][36]. The heat transfer coefficients h_c and h_r were not directly perturbed,
466 since they were calculated from T_{si}, T_i, ε , which are the input quantities considered for the implementation of
467 the Monte Carlo simulation. MCM was applied to each of the three-time windows analysed (I, II, III)
468 considering both the values of h_c defined by ASHRAE and Wilkers. In the Comfort Eye model, the generated
469 distribution for ε is only taken into account in the equation 4, as the emissivity uncertainty has been evaluated
470 in previous studies to calculate the measurement uncertainty of the IR sensor of the Comfort Eye
471 [33][36]. Thus, the uncertainty of ε is already included in the uncertainty of the input parameter T_{si} . For clarity,
472 the surface temperature values used by the Comfort Eye tool are retrieved automatically from a MySQL
473 database (Figure 2) where the correction of the emissivity according to the equation 8 is already applied. The
474 procedure used for Comfort Eye was also applied to the HFM reference method for each time window. In this
475 case, the input variables were the heat flux measured by the HFP01 sensor with an uncertainty of 3% with $k=2$
476 [35] and the T_i and T_e temperatures measured by the Type T thermocouple with an uncertainty of ± 0.5 °C.
477 Also in this case, a Gaussian distribution was used for T_i, T_e, q . This approach ensures an accurate and
478 comprehensive analysis of the data, improving the robustness and reliability of the results. The results obtained
479 from the computation performed are summarised in the Tables below.

480 In Table 3, the uncertainties for each variable are reported as standard deviations, along with their associated
481 distributions for both Comfort Eye and HFM models. All distributions were generated with a mean equal to 0,
482 and the sample from the distribution was added to the value used in the reference condition during the
483 calculation.

484

485

Table 3 Input Variables with standard deviation and distribution for both, Comfort Eye and HFM Model.

Comfort Eye			HFM		
Input Variable	$u(x_i)$	Distribution	Input Variable	$u(x_i)$	Distribution
T_{si}	$\pm 1K$	Gaussian	Heat Flux (q)	$\pm 3\%$	Gaussian
T_i	$\pm 0.5 K$	Gaussian	T_i	$\pm 0.5 K$	Gaussian
T_e	$\pm 0.5 K$	Gaussian	T_e	$\pm 0.5 K$	Gaussian
ε	± 0.014	Rectangular	/	/	/

487

488 Table 4 reports the values obtained with MCM for the measurements performed using Comfort Eye with the
 489 value of h_c defined by ASHRAE in the time windows I, II, and III (Figure 5, Figure 6, Figure 7). The values of
 490 $u_i(y)$ are expressed in $[\frac{W}{m^2K}]$ while those of $c(x_i)$ are expressed in $[\frac{W}{m^2K^2}]$ for T_{si}, T_i, T_e and in $[\frac{W}{m^2K}]$ for ε .

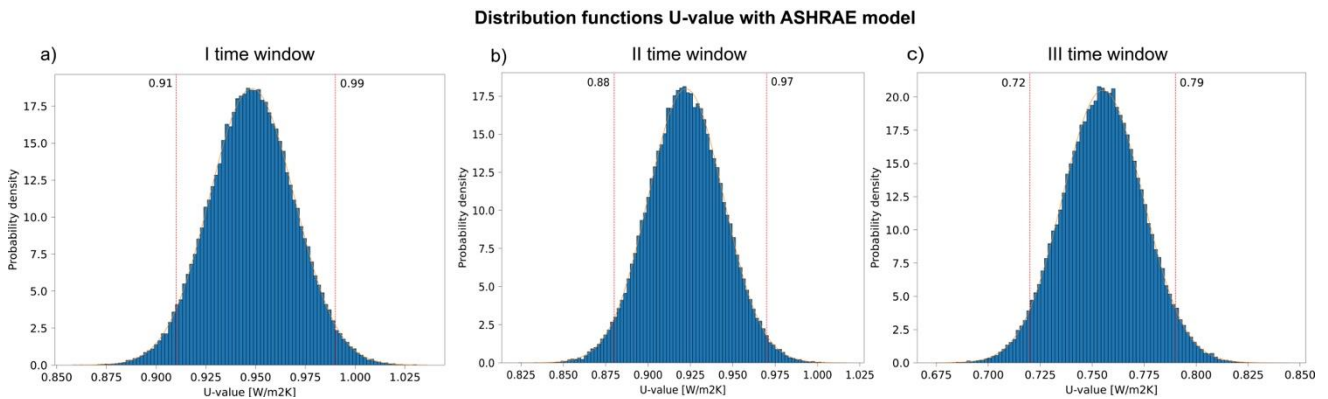
491

Table 4 Output of the Monte Carlo Analysis – Comfort Eye (ASHRAE)

h_c ASHRAE	Window I		Window II		Window III	
	$u_i(y)$	$c(x_i)$	$u_i(y)$	$c(x_i)$	$u_i(y)$	$c(x_i)$
T_{si}	0.01	0.02	0.01	0.02	0.01	0.02
T_i	0.008	0.02	0.008	0.02	0.007	0.016
T_e	0.001	0.003	0.001	0.003	0.001	0.002
ε	0.002	0.01	0.002	0.012	0.001	0.01

492

493 The Monte Carlo simulation provided an expanded uncertainty of $\pm 0.04, \pm 0.044$ and $\pm 0.04 W/m^2K$ with $k=2$
 494 on the U-value measurements in time windows I, II, III, respectively. Figure 10 shows the representation of the
 495 distribution functions of the U-value derived from the Monte Carlo simulation when all the inputs are perturbed
 496 with their measurement uncertainty. The 95% confidence interval is respectively of 0.08, 0.088 and 0.08
 497 W/m^2K for the three time windows considered.



498

Figure 10 Representation of the distribution function for the U-value measured with the IR sensor with ASHRAE model

499

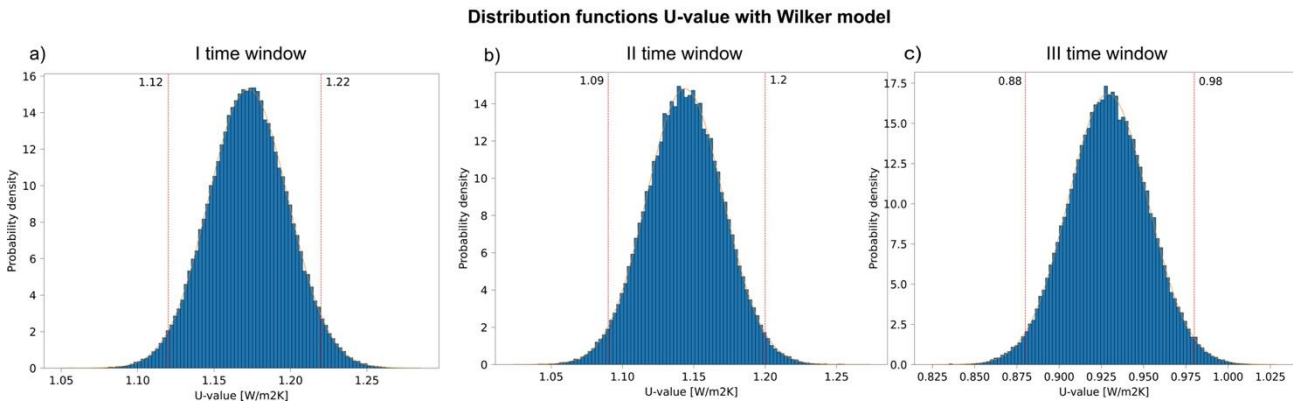
500 Table 5 reports the values obtained with MCM for the measurements performed using Comfort Eye with the
 501 value of h_c defined by Wilkers in time windows I, II, and III, respectively. The values of $u_i(y)$ are expressed
 502 in $[\frac{W}{m^2K}]$ while those of $c(x_i)$ are expressed in $[\frac{W}{m^2K^2}]$ for T_{si}, T_i, T_e and in $[\frac{W}{m^2K}]$ for ϵ .

503 *Table 5 Output of the Monte Carlo Analysis- Comfort Eye (Wilkers)*

h_c Wilkers	Window I		Window II		Window III	
Input Variables	$u_i(y)$	$c(x_i)$	$u_i(y)$	$c(x_i)$	$u_i(y)$	$c(x_i)$
T_{si}	0.02	0.024	0.02	0.024	0.02	0.021
T_i	0.01	0.021	0.01	0.021	0.01	0.02
T_e	0.001	0.003	0.001	0.003	0.001	0.002
ϵ	0.002	0.012	0.002	0.012	0.001	0.01

504

505 The Monte Carlo simulation for Comfort Eye provided an expanded uncertainty of ± 0.05 , W/m²K with k=2
 506 on the U-value measurements in time windows I, II III. Figure 11 shows the representation of the distribution
 507 functions of the U-value derived from the Monte Carlo simulation when all the inputs are perturbed with their
 508 measurement uncertainty. The 95% confidence interval is equal to 0.1 W/m²K for the three time windows
 509 considered.



510 *Figure 11 Representation of the distribution function for the U-value measured with the IR sensor with Wilkers model*

511 Table 6 reports the values obtained with MCM for the measurements performed with the HFM for time
 512 windows I, II, and III. The values of $u_i(y)$ are expressed in $[\frac{W}{m^2K}]$ while those of $c(x_i)$ are expressed in $[\frac{W}{m^2K^2}]$
 513 for T_i, T_e and in $[\frac{1}{K}]$ for q .

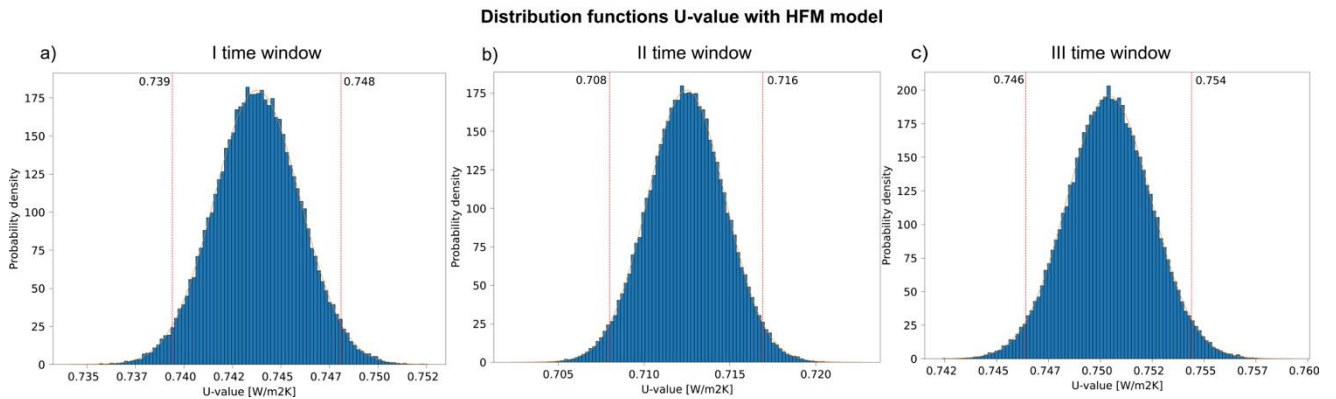
514 *Table 6 Output of the Monte Carlo Analysis- HFM*

HFM	Window I		Window II		Window III	
Input Variables	$u_i(y)$	$c(x_i)$	$u_i(y)$	$c(x_i)$	$u_i(y)$	$c(x_i)$
Heat Flux (q)	0.001	0.003	0.001	0.003	0.001	0.002

T_i	0.001	0.002	0.001	0.002	0.001	0.002
T_e	0.001	0.002	0.001	0.002	0.001	0.002

515

516 The Monte Carlo simulation for the HFM method provided an expanded uncertainty of ± 0.004 W/m²K with
517 $k=2$ on the U-value measurements in time windows I, II, III, respectively. Figure 12 shows the representation
518 of the distribution functions of the U-value derived from the Monte Carlo simulation when all the inputs are
519 perturbed with their measurement uncertainty. The 95% confidence interval is of 0.008 W/m²K for all three
520 the time windows.



521

Figure 12 Representation of the distribution function for the U-value measured with the HFM model

522 To understand the actual applicability of the approach proposed under real environmental conditions, an
523 additional variance-based sensitivity analysis was performed to test the hypothesis of uncorrelated inputs for
524 the Comfort Eye approach. The sensitivity analysis was carried out by considering the influence of the input
525 parameters.

526 The general procedure consists in calculating the first order sensitivity indexes (S_i) according to the method
527 described in [38], which is a variance-based method:

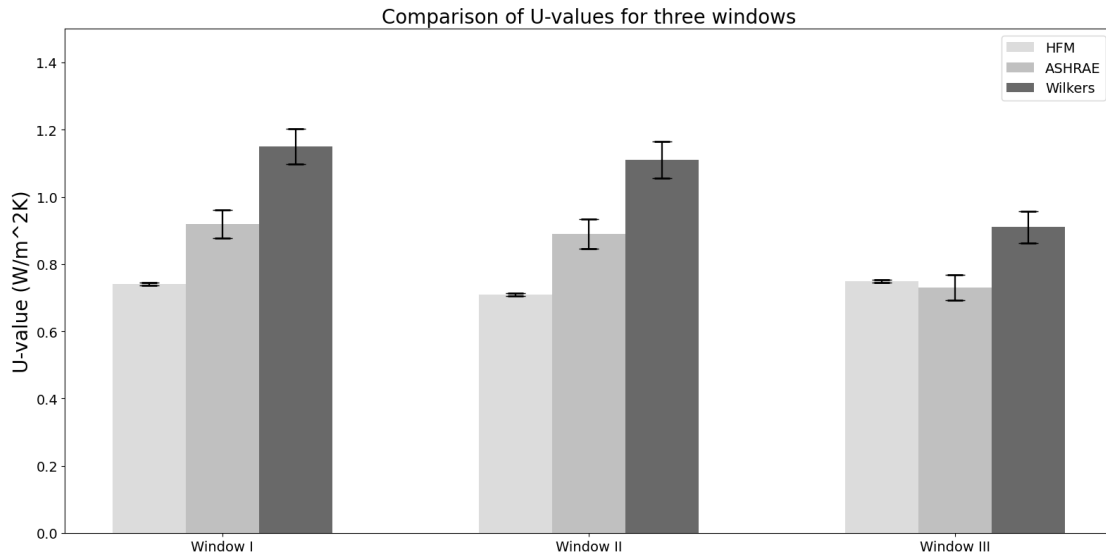
$$S_i = \frac{V_{x_i}}{V_{tot}} \quad (9)$$

528 where V_{x_i} is the output variance when considering as input only the random distribution of the parameter x_i
529 while keeping the other parameters constant, and V_{tot} is the total variance of the output due to the perturbation
530 of the model when considering as input the random distribution of all the inputs. Thus, each index can be
531 represented as a percentage of the total variance of the output. As a result, the sum of all the S_i is equal to 98%,
532 which is near to unity (100%). This demonstrates that only minor correlations are present, and inputs can be
533 considered as being uncorrelated with a negligible impact on the uncertainty analysis.

534

6.2 Discussion of the results

535 The uncertainty of the method proposed was evaluated through Monte Carlo simulations. The following figure
 536 shows the results in terms of mean and standard deviations of the uncertainty analysis for the IR model with
 537 the values of h_c defined by Wilkers and ASHRAE and for the HFM reference method in the three-time
 538 windows.

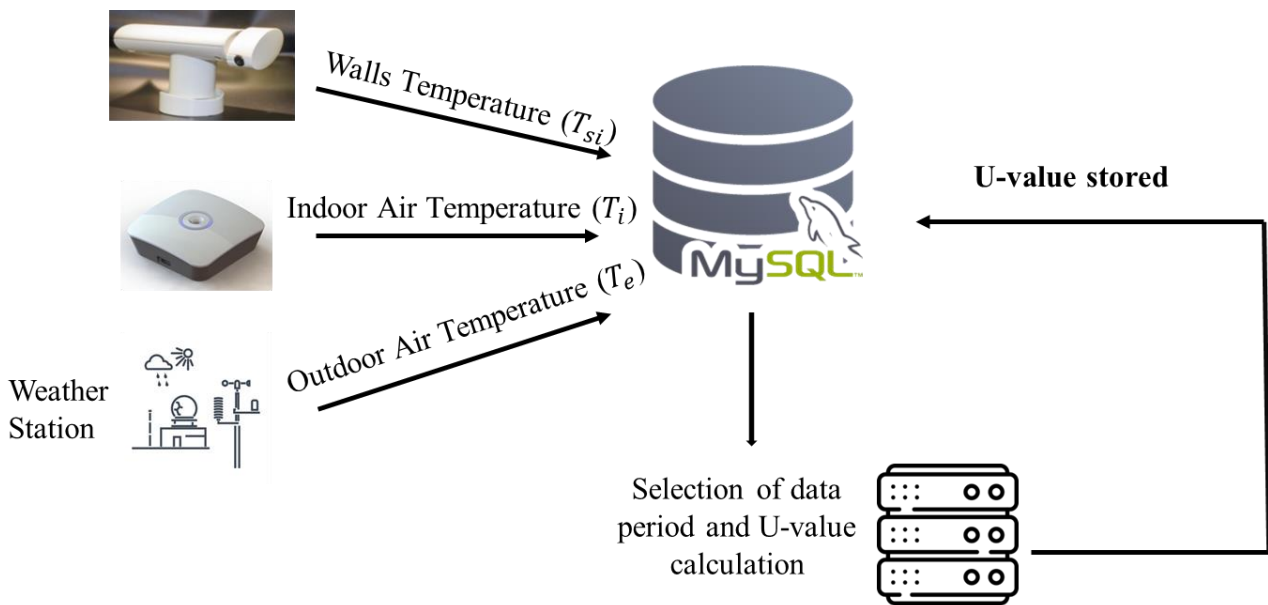


539 *Figure 13 Mean and Standard deviations with $k=2$ for the IR model with the values of h_c defined by ASHRAE and*
 540 *Wilkens and for the HFM model in the three time windows*

541 **6.3** The figure (Figure 13) presented in this section clearly illustrates how the choice of the h_c
 542 coefficient can significantly impact U-value measurements. Moreover, the results indicate that the
 543 measurement accuracy is highly dependent on operating conditions. Concerning the impact of the
 544 input uncertainty, the most accurate result for the IR model (Comfort Eye) was obtained in time
 545 window III using the value of h_c defined by ASHRAE. In this time window, the mean and standard
 546 deviation values for the HFM, ASHRAE, and Wilkers methods were respectively 0.75 ± 0.004 , 0.73
 547 ± 0.04 , and 0.91 ± 0.05 W/m²K with $k=2$. It is worth noting that in time window III the temperature
 548 difference was greater than 10°C for more than 50% of the time, as shown in Figures 5, 6, and 7.
 549 Moreover, a systematic deviation on the final U-value between the HFM and IR model was found in
 550 all the time windows. In particular, such deviation was higher for window I and II, when the
 551 conditions required by the standard are not completely satisfied. Therefore, such deviation should be
 552 corrected when using the IR model. In this particular case, considering the ASHRAE model, the
 553 correction factors are -0.18, -0.18 and +0.02 W/m²K for the three time windows, respectively. These
 554 findings suggest that the selection of an appropriate time window for the measurements is crucial
 555 and should, therefore, be taken into careful consideration. Overall, the methodology proposed can
 556 serve as a useful tool for U-value estimation without the need for extra measuring tools. However,
 557 further research is necessary to validate the methodology under different operating conditions and
 558 for different building types. **Guideline for application**

559 Considering the results reported and the functionalities of Comfort Eye, the system not only provides an
 560 analysis of indoor environmental conditions, particularly regarding thermal comfort and air quality, but it also
 561 allows the analysis of the thermal performance of a wall. The calculation of the heat transfer coefficient (U-
 562 value) is more accurate with a temperature difference between interior and exterior environments greater than
 563 10 °C for a period exceeding 50% of the time. Based on this premise, Comfort Eye allows real time monitoring
 564 for long periods and the storage of the data collected in the MySQL database, therefore it makes it possible to
 565 select among the data collected those that meet the standard requirements. When using the Comfort Eye
 566 system, should it not be possible to install a sensor to measure external temperature, the necessary data can be
 567 extracted from an external weather station via an API service.

568 Once the data are selected, the heat transfer coefficient model can be applied to provide an analysis of the
 569 thermal performance of the wall (Figure 14). As the system can be installed for long periods, this process can
 570 be repeated multiple times to evaluate changes in the thermal performance over time.



571

572 *Figure 14 Workflow for U-value calculation using Comfort Eye and weather data. The model makes it possible to*
 573 *select the time window with a temperature difference between the interior and exterior environments greater than 10 °C*

574

575

576 **7. Conclusions**

577 A method for U-value in-situ experimental determination based on the measurement of indoor surface
578 temperature using an IoT, non-contact, full-field IR sensor was proposed. Comfort Eye, a system for the
579 evaluation of IEQ which is equipped with an IR sensor, was adopted to measure the inside surface temperature
580 of a façade wall. The method was validated through a test in a real environment and the measurements were
581 taken according to ISO 9869-1 and ISO 9869-2 procedures.

582 This paper shows that the method proposed for U-value calculation under realistic environmental conditions
583 is reliable. In the case presented, the outcomes demonstrated that the best result is obtained with the heat
584 transfer coefficient h_c reported by ASHRAE and a ΔT between indoor and outdoor air temperature greater than
585 $10\text{ }^\circ\text{C}$ for at least 50 % of the time, which is in line with the requirements of ISO 9869-2. Different time
586 windows were analysed to demonstrate the repeatability of the methodology applied. When monitoring in real
587 environmental conditions, however, this requirement could be a limitation. The Comfort Eye sensor makes it
588 possible to overcome this limitation by performing long-term monitoring and selecting only time-windows
589 with a ΔT greater than 10°C .

590 The paper also illustrated the application of MCM to analyse the measurement uncertainty of thermal
591 transmittance using the IR system (Comfort Eye). The aim is to identify the measurement uncertainty of the
592 U-value by applying the GUM guidelines and the Monte Carlo method to define the impact of the measurement
593 uncertainty of the sensors used to monitor the data necessary to calculate the U-value. The results obtained
594 indicate that the measurement accuracy is highly dependent on operating conditions. The most accurate result
595 for the IR model was obtained using the value of h_c defined by ASHRAE in time window III. In this time
596 window, the mean and standard deviation values for the HFM, ASHRAE, and Wilkers methods were
597 respectively 0.75 ± 0.004 , 0.73 ± 0.04 , and $0.91 \pm 0.05\text{ (W/m}^2\text{K)}$ with $k=2$. It is worth noting that in time
598 window III the temperature difference was greater than 10°C for more than 50% of the time, as shown in
599 Figures 5, 6, and 7. These findings suggest that the choice of an appropriate time window for the measurements
600 is crucial and should, therefore, be taken into careful consideration. The results showed that different
601 environmental quantities produce different uncertainties of the U-value. T_{si} contributed the most to this
602 uncertainty, since $U(T_{si}) = \pm 1\text{ }^\circ\text{C}$. The variance-based sensitivity analysis demonstrates that the input
603 parameters can be considered as being uncorrelated.

604 In conclusion, the methodology provides an innovative solution for the measurement of the indoor surface
605 temperature of a wall in a built environment, making it possible to determine the U-value. It is important to
606 underline that the uncertainty values estimated in this analysis should not be considered as the absolute
607 uncertainty of the tool but rather as the discrepancy with respect to the reference HFM model, which, in
608 addition, includes its own component of uncertainty. The final result is that the IR system presents a confidence
609 interval of the measured U-value that is one order of magnitude higher than the one achieved with the HFM
610 system.

611 Thanks to its ability to perform real-time and continuous monitoring and for long periods, Comfort Eye has
612 the capability to identify changes in surface heat over time. Therefore, the thermal dynamic behaviour of a
613 whole wall can be available in real-time. Even under real environmental conditions, the calculation of thermal
614 transmittance using the IR method showed good accuracy. Thermal bridges can affect the accuracy of U-value
615 measurements and for this reason further analyses will be considered in future investigations in order to
616 understand how much the selection of the ROI could affect the thermal transmittance measurements.

617

618 **Data availability**

619 The data that support the findings of this study are available upon request from the authors.

620 **References**

621

- 622 [1] A. Tahmassebia, A. H. Gandomib, “Building energy consumption forecast using multi-objective
623 genetic”, *Measurement* 118 (2018) 164–171.
- 624 [2] I. Jabłon´ ski “Integrated living environment: Measurements in modern energy efficient smart building
625 with implemented the functionality of telemedicine” *Measurement* 101 (2017) 211–235.
- 626 [3] Principi, P., Roberto, F., Carbonari, A., & Lemma, M. (2016). Evaluation of energy conservation
627 opportunities through Energy Performance Contracting: A case study in Italy. *Energy and Buildings*,
628 128, 886-899.
- 629 [4] T. Kurczveil, P. Diekhake, J. Liu, E. Schnieder, “Consumer load measurement in automated buildings”,
630 *Measurement* 51 (2014) 441–450.
- 631 [5] M. Nilashi, M. Dalvi-Esfahani, O. Ibrahim, K. Bagherifard, A. Mardani, N. Zakuan “A soft computing
632 method for the prediction of energy performance of residential buildings”, *Measurement* 109 (2017)
633 268–280.
- 634 [6] Guo, M., Zhou, M., Wei, S., Peng, J., Wang, Q., Wang, L., Cheng, D., & Yu, W. (2021). Particle removal
635 effectiveness of portable air purifiers in aged-care centers and the impact on the health of older people.
636 *Energy and Buildings*, 250, 111250.
- 637 [7] Park H, Martaj N, Ruellan M, Bennacer R, Monmasson E. Modeling of a Building System and its
638 Parameter Identification [Internet]. Vol. 8, *Journal of Electrical Engineering and Technology*. The
639 Korean Institute of Electrical Engineers; 2013. p. 975–83
- 640 [8] EN ISO 6949, Building components and building elements – Thermal resistance and Thermal
641 transmittance – Calculation method, 2007.
- 642 [9] ISO 8990, Thermal insulation - Determination of steady-state thermal transmission properties -
643 Calibrated and and guarded hot box, 1994
- 644 [10] ISO 9869-1, Thermal insulation – Building elements – In-situ measurement of thermal resistance and
645 Thermal transmittance – Part 1: Heat flow meter method, 2014.
- 646 [11] X. Meng, T. Luo, Y. Gao, L. Zhang, Q. Shen and E. Long, "A new simple method to measure wall

- 647 thermal transmittance in situ and its adaptability analysis", *Applied Thermal Engineering*, vol. 122, p.
648 747–757, 2017.
- 649 [12] K. Gałażka, S. Populoh, W. Xie, J. Hulliger, A. Weidenkaff "Radiative heat losses in thermal
650 conductivity measurements: a correction for linear temperature gradients", *Measurement* 90 (2016)
651 187–191.
- 652 [13] A. Rasooli, L. Itard, "In-situ characterization of walls' thermal resistance: An extension to the ISO
653 9869 standard method" *Energy & Buildings* 179 (2018) 374–383
- 654 [14] M. Cucumo, A. De Rosa, V. Ferraro, D. Kaliakatsos and V. Marinelli, "A method for the experimental
655 evaluation in situ of the wall conductance," *Energy and Buildings*, vol. 38, pp. 238-244, 2006.
- 656 [15] R. Albatici and A. M. Tonelli, "Infrared thermovision technique for the assessment of thermal
657 transmittance value of opaque building elements on site", *Energy and Buildings*, vol. 42, pp. 2177-2183,
658 2010.
- 659 [16] R. Albatici, A. M. Tonelli and M. Chiogna, "A comprehensive experimental approach for the
660 validation of quantitative infrared thermography in the evaluation of building thermal transmittance",
661 *Applied Energy*, vol. 141, pp. 218-228, 2015.
- 662 [17] A. G. Mainini, T. Poli, R. Paolini, M. Zinzi and L. Vercesi, "Transparent multilayer ETFE panels for
663 building envelope: thermal transmittance evaluation and assessment of optical and solar performance
664 decay due to soiling", in SHC 2013, *International Conference on Solar Heating and Cooling for*
665 *Buildings and Industry*, Freiburg, Germany, 2013.
- 666 [18] Ohlsson, K.E.A. and T. Olofsson, Quantitative infrared thermography imaging of the density of heat
667 flow rate through a building element surface. *Applied Energy*, 2014. 134: p. 499-505.
- 668 [19] Fokaides, P.A. and S.A. Kalogirou, Application of infrared thermography for the determination of the
669 overall heat transfer coefficient (UValue) in building envelopes. *Applied Energy*, 2011. 88(12): p. 4358-
670 4365.
- 671 [20] I. Danielski and M. Fröling, "Diagnosis of buildings' thermal performance - a quantitative method
672 using thermography under non-steady state heat flow", in *7th International Conference on*
673 *Sustainability in Energy and Buildings*, Lisbon, Portugal, 2015.
- 674 [21] M. Teni, H. Krstić, P. Kosiński, Review and comparison of current experimental approaches for in-
675 situ measurements of building walls thermal transmittance, *Energy and Buildings*, Volume 203, 2019.
- 676 [22] D. B-Huertas, J.Moyano, D. Marín, R. F.Contreras, Review of in situ methods for assessing the
677 thermal transmittance of walls, *Renewable and Sustainable Energy Reviews*, Volume 102, 2019,Pages
678 356-37
- 679 [23] ISO 9869-2, Thermal insulation- Building elements In-situ measurement of thermal resistance and
680 thermal transmittance – Infrared method for frame structure dwelling, 2018.
- 681 [24] S.Serroni, M. Arnesano, G. Pandarese, M.Martarelli, G.M. Revel, IoT infrared sensor for continuous
682 monitoring of building envelope thermal performances, *Splitech* 2021
- 683 [25] S.Serroni, M. Arnesano, M.Martarelli, G.M. Revel, Application of an IoT infrared sensor for thermal

- 684 transmittance measurement in building renovation, Splitech 2022
- 685 [26] BIMSPEED Project : <https://www.bim-speed.eu/en>
- 686 [27] GUM - JCGM 101, Evaluation of measurement data - Supplement 1 to the “Guide to the expression
687 of uncertainty in measurement” — Propagation of distributions using a Monte Carlo method, 2008
- 688 [28] Fokaides, P. A., & Kalogirou, S. A. (2011). Application of infrared thermography for the determination
689 of the overall heat transfer coefficient (U-Value) in building envelopes. *Applied Energy*, 88(12), 4358-
690 4365.
- 691 [29] Usamentiaga R, Venegas P, Guerediaga J, Vega L, Molleda J, Bulnes FG. Infrared thermography for
692 temperature measurement and non-destructive testing. *Sensors (Basel)*. 2014 Jul 10;14(7):12305-48.
- 693 [30] Acikgoz, O.; Kincay, O. Experimental and numerical investigation of the correlation between radiative
694 and convective heat-transfer coefficients at the cooled wall of a real-sized room. *Energy Build*. 2015,
695 108, 257–266.
- 696 [31] Antunovi´c, B.; Stankovi´c, M.; Jankovi´c, A.; Gaji´c, D.; Todorovi´c, D. Measurement of thermal
697 transmittance in the Rectorate building of the University of Banja Luka. In *Proceedings of the*
698 *International Scientific Conference Contemporary Theory and Practice in Civil Engineering*, Banja
699 Luka, Bosnia and Herzegovina, 26–27 April 2012; pp. 37–46
- 700 [32] M. Gaši , B. Milovanovi´, S. Gumbarevi, "Comparison of Infrared Thermography and Heat Flux
701 Method for Dynamic Thermal Transmittance Determination, *Buildings* 2019, 9, 132;
- 702 [33] G.M.Revel, M. Arnesano, F.Pietroni, “Development and validation of a low-cost infrared
703 measurement system for real-time monitoring of indoor thermal comfort”, *Measurement Science and*
704 *Technology* 25 (2014) 085101 (10pp)
- 705 [34] S.Serroni, M.Arneseano, L.Violini, G.M.Revel, A IoT measurement solution for continuous indoor
706 environmental quality monitoring for buildings renovation., *Acta Imeko*, Vol. 10 2021
- 707 [35] [https://www.hukseflux.com/products/heat-flux-sensors/heat-flux-sensors/hfp01-heat-flux-](https://www.hukseflux.com/products/heat-flux-sensors/heat-flux-sensors/hfp01-heat-flux-sensor)
708 [sensor](https://www.hukseflux.com/products/heat-flux-sensors/heat-flux-sensors/hfp01-heat-flux-sensor)
- 709 [36] Lorenzo Zampetti, Development of a low-cost system for thermal comfort measurement and
710 control. PhD Thesis, 2017
- 711 [37] N.Morresi, S.Casaccia,M.Arneseano, G.M.Revel, Impact of the measurement uncertainty on the
712 monitoring of thermal comfort through AI predictive algorithms., *Acta Imeko*, Vol. 10 2021
- 713 [38] Saltelli, A., Ratto, M., Andres, T., Campolongo, F., Cariboni, J., Gatelli, D., Saisana, M. and Tarantola,
714 S. (2007). Variance-Based Methods. In *Global Sensitivity Analysis. The Primer* (eds A. Saltelli, M.
715 Ratto, T. Andres, F. Campolongo, J. Cariboni, D. Gatelli, M. Saisana and S. Tarantola)

716

717

718